Available online at www.sciencedirect.com
ScienceDirect
Journal of the European Ceramic Society 29 (2009) 385–390
www.elsevier.com/locate/jeurceramsoc

Elastic properties of porous polycrystalline thoria—A relook

K.K. Phani *, Dipayan Sanyal

Central Glass & Ceramic Research Institute, 196 Raja S.C. Mullick Road, Kolkata 700032, India

Received 17 May 2007; received in revised form 30 August 2007; accepted 30 September 2007
Available online 4 October 2008

Abstract

Elastic constant–porosity relation for polycrystalline thoria reported by previous researchers has been reanalyzed on the basis of the Mori–Tanaka mean field approach and a power law dependence of moduli with porosity. It indicates that the shear modulus dependence on Young's modulus is possibly related to the sintering characteristics of the material rather than pore morphology. A new method has been suggested for predicting variations of elastic properties and porosity with the progress in sintering of thoria based on experimental data at a single porosity only. The predicted values agree with the experimental data quite well.

Keywords: ThO_2; Porosity; Elastic properties

1. Introduction

Ceramic materials are usually prepared by sintering green powder compacts. This invariably leaves some amount of porosity in the material. Thus ceramists studying the relation between microstructure and macroscopic properties have always been concerned with the effect of porosity on macroscopic properties—in particular the effect of porosity on elastic properties. In an effort to develop the elastic moduli–porosity relations for polycrystalline material, Spinner et al.[1] made a detailed study of porous polycrystalline thoria. One of the reasons for choosing thoria for their study was that being a cubic crystal its thermal expansion was isotropic and therefore, thermally induced intergranular stresses which might be present in other type of crystals were not present. So it was expected that the porosity–elastic moduli relationship developed based on the study of thoria would come closer to the "ideal" situation. Spinner et al.[1] prepared three groups of samples designated as Groups I, II and III. In Group I specimens, the particle size was in the range 0–2 μm and to prepare specimens of porosity greater than ≈8%, 6–40% volume fraction of unsulfonated styrene-divinyl benzene beads (250–325 mesh) were used as an artificial pore former. For Group II specimens, particle size was 2–4 μm and 6–36% of the same pore former was used to prepare specimens above ≈12% porosity. Group III specimens were prepared without any pore former with particle size 4–44 μm. Each of the four specimens in this group were prepared by using different powder sizes. The porosity of first two groups varied between 3% and ≈40% whereas for the third group it was in the range ≈17% and ≈26%. The shear modulus and Young's modulus of the sintered samples were measured by the dynamic resonance method and other elastic constant values namely the bulk modulus and Poisson's ratio were calculated from these measured values by using well known relations given by the theory of elasticity. They analyzed their experimental data of elastic moduli in terms of an empirical equation given by a second degree polynomial in porosity. For both Young's and shear moduli of Groups I and II specimens the equation gave two sets of different curves showing larger decrease in moduli with porosity for Group I specimens. The data for Group III specimens gave satisfactory agreement with the equations developed for Group II. Also the relative decrease in Young's modulus was greater than the relative decrease in the shear modulus by a larger amount for Group I specimens than for Groups II and III specimens. As a result Poisson's ratio for Group I showed greater decrease with porosity than that of Groups II and III.

They also analyzed their experimental data on the basis of theoretical expressions given by various researchers[2–6] and found that the relative decrease in elastic moduli obtained experimentally was greater than what theoretical equations predict. This

* Corresponding author.
E-mail address: kkphani@cgcri.res.in (K.K. Phani).

0955-2219/$ – see front matter © 2008 Published by Elsevier Ltd.
doi:10.1016/j.jeurceramsoc.2007.09.055

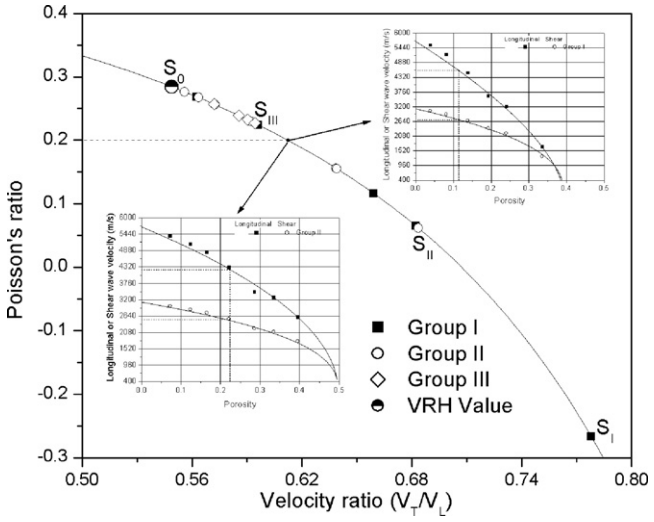

Fig. 1. Variation of the shear modulus of Groups I, II and III specimens with Young's modulus. The solid line corresponds to Eq. (11) with $n_0 = 0.412$.

deviation was attributed to the non-sphericity of pores in the specimens. Since the decrease in moduli with porosity for Group I specimens was more than that of Group II or III specimens, it was concluded that the pores of the specimens of Group I should depart from being spherical to a greater degree than those of Group II or III.

The Poisson's ratio of Group I specimen having the highest porosity of 33.40% was negative and Spinner et al.[1] considered this to be an erroneous data though it was in line with the trend of variation of Poisson's ratio with porosity for Group I specimens derived by them. It may be noted that the isotropic elastic theory[7] allows negative Poisson's ratios, with limits of ν given by $-1 < \nu < 0.5$ and for few cases of isotropic and homogeneous material negative Poisson's ratio has been reported in the literatures[8–10]. Dean[11] has also analyzed the data for Groups I and II specimens using a variable aspect ratio self-consistent oblate spheroidal inclusion theory given by Wu[12] and obtained the "effective" aspect ratio of pores as 0.241 and 0.475 for Groups I and II, respectively. Though the theory explained the elastic moduli variation with porosity quite well, it failed in case of Poisson's ratio. This was attributed to the overestimation of the value of Poisson's ratio by the theory for porosities above 30%.

Fig. 1 shows a plot of the shear modulus of these three groups of data against their Young's modulus. It apparently contradicts some of the observations regarding the effect pore morphology on elastic moduli made by the previous researchers[1,11] and indicates that the variation of shear moduli with Young's moduli of all the groups of data can possibly be described by a single equation (which is derived later) given by the solid line with ±5% accuracy even though they have different starting powder sizes and pore morphologies.

In this paper we present an analysis of the data from a different view point. First we derive a relation between the shear and Young's modulus using self-consistent theory based on the Mori–Tanaka mean field approach[13] to explain the variation of the shear modulus with Young's modulus and then present a new method of predicting the variation of elastic moduli with porosity using the experimentally measured data at a single point corresponding to the highest porosity in each group. We also attempt to address the issue whether it is the porosity or some other parameter which explains the observed behaviour better.

2. Analytical derivation

2.1. The shear modulus and young's modulus relation

The effective bulk (K) and shear (G) moduli of a porous solid containing spheroidal shaped pores can be derived from Mori–Tanaka approach as[14]

$$K = \frac{K_0}{1 + pf(\nu_0, \alpha)/(1-p)} \tag{1}$$

$$G = \frac{G_0}{1 + ph(\nu_0, \alpha)/(1-p)} \tag{2}$$

where K_0, G_0 and ν_0 are bulk modulus, shear modulus and Poisson's ratio of pore-free material, respectively and α is the aspect ratio of the spheroidal pores and p is the porosity. $f(\nu_0, \alpha)$ and $h(\nu_0, \alpha)$ are the functions of ν_0, α and for simple explicit forms of these functions reference may be made to the Appendix of the reference[14]. Using the relation between K, G and Poisson's ratio, ν, for isotropic elastic solids[7], i.e.

$$\nu = \frac{3K - 2G}{6K + 2G} \tag{3}$$

and Eqs. (1) and (2), expression for Poisson's ratio of porous solid is obtained as[14]

$$\nu = \frac{3\nu_0(1-p) - pf(\nu_0, \alpha)(1-2\nu_0) + ph(\nu_0, \alpha)(1+\nu_0)}{3(1-p) + pf(\nu_0, \alpha)(1-2\nu_0) + 2ph(\nu_0, \alpha)(1+\nu_0)} \tag{4}$$

For isotropic material E and G are related by the equation[7]

$$G = \frac{E}{2(1+\nu)} \tag{5}$$

which in terms of normalized moduli values can be written as

$$\frac{G}{G_0} = \frac{1+\nu_0}{1+\nu}\frac{E}{E_0} \tag{6}$$

Substitution of Eq. (4) in Eq. (6) and on simplification gives

$$\frac{G}{G_0} = \left[1 + \frac{((1-2\nu_0)p/3)(f(\nu_0, \alpha) - h(\nu_0, \alpha))}{1 + p(h(\nu_0, \alpha) - 1)}\right]\frac{E}{E_0} \tag{7}$$

Substituting values of $f(\nu_0, \alpha)$ and $h(\nu_0, \alpha)$ in terms G,G_0, K, K_0 and p from Eqs. (1) and (2) and using the relation $E = 9KG/(3K+G)$ from the theory of elasticity[7], Eq. (7) reduces to

$$\frac{G}{G_0} = \left[\frac{2}{3}(1+\nu_0) + \frac{1-2\nu_0}{3}\frac{E}{E_0}\lambda(K, G)\right]\frac{E}{E_0} \tag{8}$$

where λ is a function of K_0, G_0, K, G and is given by

$$\lambda(K, G) = \frac{K_0(3 + G/K)}{K(3 + G_0/K_0)} \tag{9}$$

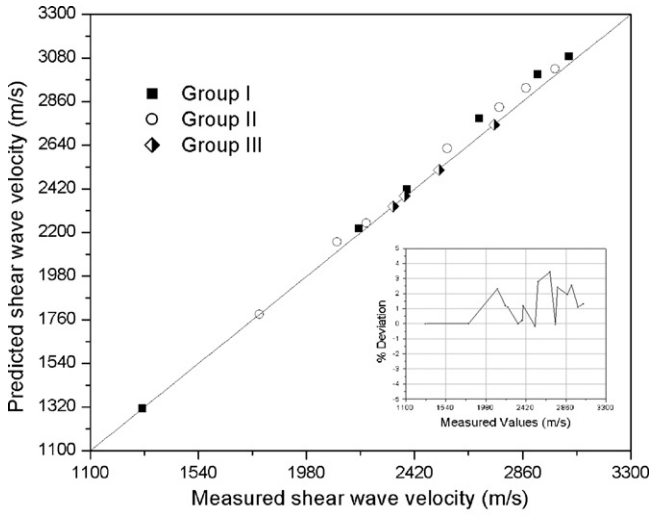

Fig. 2. A plot of $\lambda(K,G)$ vs. E/E_0 for Groups I, II and III specimens.

Eq. (9) shows that G/G_0 can be expressed explicitly in terms of E/E_0 if the function $\lambda(K,G)$ can be expressed as a function E/E_0. Analytically $\lambda(K,G)$ cannot be expressed as a function of E/E_0. To ascertain whether any relation at all exists between $\lambda(K,G)$ and E/E_0, we plotted $\lambda(K,G)$ values against E/E_0 for all the three groups of data, which is shown in Fig. 2. Fig. 2 shows that the function $\lambda(K,G)$ can possibly be expressed as a hyperbolic function of E/E_0. A non-linear regression analysis yielded the relation $\lambda(K,G)\,(E/E_0)^{1.075} = 1$ with a R-squared value of 0.994. Thus we assume the functional form of the relation between $\lambda(K,G)$ and E/E_0 as

$$\lambda(K, G) = \frac{1}{(E/E_0)^n} \tag{10}$$

where n is a constant for a given porous material.

Combining Eqs. (8) and (10) and simplifying gives

$$G = \left[\frac{2}{3}(1+\nu_0)\frac{E}{E_0} + \frac{1-2\nu_0}{3}\left(\frac{E}{E_0}\right)^{n_0}\right] G_0 \tag{11}$$

where $n_0 = 2 - n$ is a constant for a given porous material. Comparison of Eq. (7) with Eq. (11) indicates that parameter n_0 is possibly related to the pore morphology of the material. Eq. (11) shows that if the pore-free elastic moduli values (i.e. E_0, G_0 and ν_0) are known from the mean polycrystalline (VRH) values or otherwise, the value of n_0 can be evaluated by knowing the E and G values at a single porosity value only.

2.2. Porosity dependence of elastic moduli

The variation of elastic moduli with porosity is usually analyzed in terms of a power law equation[15] given by

$$M = M_0(1 - ap)^{n_X} \tag{12}$$

where M stands for E or G; n_x and a are constants, p is the porosity and $X = E$ or G for Young's and shear moduli, respectively. The constant 'a' is related to the critical porosity (p_c) at which elastic moduli vanishes, by the relation $a = 1/p_c$. The value of p_c can only be in the range $0 < p_c \leq 1$, therefore minimum value of a is 1.

The right hand side of Eq. (12) contains two unknowns 'a' and n_x and to determine the value of n_x uniquely at least $n_x + 1$ data point's values must be known. Moreover values of E and G calculated from Eq. (12) must satisfy Eq. (11). Therefore a relation correlating M, n_x, a and n_0 is derived as follows:

$$\frac{dG}{dE} = \frac{dG}{dp}\frac{dp}{dE} \tag{13}$$

Evaluating the left hand hide from Eq. (11) and the right hand side from Eq. (12) and substituting in Eq. (13) gives after mathematical simplification

$$\Gamma = n_G\left(\frac{G}{G_0}\right)^{((n_G-1)/n_G)} \tag{14}$$

where

$$\Gamma = n_E\left(\frac{2(1+\nu_0)}{3} + \frac{n_0(1-2\nu_0)}{3}\left(\frac{E}{E_0}\right)^{n_0-1}\right)\left(\frac{E}{E_0}\right)^{((n_E-1)/n_E)} \tag{15}$$

Eq. (14) shows that a Ln–Ln plot of Γ versus G/G_0 should give a straight line and the value of n_G can be obtained from the antilogarithm of the intercept on Ln (Γ) axis. However, to evaluate Γ, n_E and $(n_E + 1)$ number values of E with corresponding values of G must be known. Thus the following procedure is adopted to find the values of n_E, n_G and 'a' from Eqs. (11), (14) and (15).

First n_0 is evaluated from Eq. (11) using experimentally measured E and G values at a single porosity. For the values of E_0 and G_0, either mean polycrystalline (VRH) values or experimentally measured values are used. An initial estimate of n_E is made from Eq. (12) using the same experimental values as is used in estimation of n_0, taking the value of $a = 1$. A set of ten E values including E_0 are then generated by dividing Young's moduli values between E_0 and zero in ten equal intervals and the corresponding values of G are then calculated from Eq. (11) using n_0 value determined earlier. Using these values of E and G and initial estimate of n_E, a Ln–Ln plot of Γ versus G/G_0 is made and the linearity of the plot is checked through the value of coefficient of regression (R-squared). The value of 'a' is then incremented in steps of 0.001 giving a new estimate of n_E and Γ and a new value of R^2 is calculated from the Ln–Ln plot. The value of 'a' is taken as the value for which R^2 becomes maximum. n_G is then calculated from the intercept. A minimum value of 0.950 for the R^2 is considered as the good fit. The estimation is made on the basis of ten data points on the assumption $n_E < n_G \leq 9$. It may be mentioned here this data fitting can be easily carried out on an Excel spread sheet in conjunction with a scatter diagram.

3. Data analysis

The values of n_0 for Groups I and II data sets were evaluated from Eq. (11) using the reported[1] experimental values of E and G at highest porosities of 33.40% and 39.44%, corresponding to Groups I and Group II, respectively. The calculations were based on the VRH values $K_0 = 193$ GPa and $G_0 = 97.2$ GPa, obtained

Table 1
Summary of the parameters of Eq. (12) calculated from the highest porosity data

System	Parameters		
	a	n_E	n_G
Group I	2.725	1.121	0.913
Group II	2.053	1.087	0.959

from single-crystal elastic constants determined by Macedo et al.[16]. Corresponding values of E_0 and ν_0 are 247.7 GPa and 0.284, respectively. The values of n_0 work out to be 0.322 and 0.501 for Groups I and II data sets, respectively. Eq. (11) corresponding to these values of n_0 is shown in Fig. 1 by chain dotted and dotted lines for Groups I and II, respectively. In both cases the agreement between Eq. (11) and experimentally measured values are extremely close with the maximum deviation being 2.8% only. Group III data sets as shown in Fig. 1, closely follow the equation developed for Group II. No separate value of n_0 was evaluated for this group since no two specimens in this group had identical starting powder sizes.

Variation of the shear modulus and Young's modulus with porosity were evaluated using the procedure described above using experimental values of E at porosities of 33.40% and 39.44% and n_0 values of 0.322 and 0.501 for Group I and Group II specimens, respectively. The calculated values of a, n_E and n_G are given in Table 1. Eq. (12) corresponding to these values along with the experimental data is shown in Fig. 3 showing excellent agreement between the two. Except for the value at 28.5% porosity for Group II specimens, all the values lie within ±6% of the predicted values of moduli. As before, Group III data closely follow the equation given for Group II.

Fig. 4 shows the comparison of predicted values of the bulk moduli with the experimentally measured ones plotted against porosity. The predicted bulk moduli values with porosity were obtained by combining Eq. (11) with the well known relation[7]

$$K = \frac{EG}{3(3G - E)} \tag{16}$$

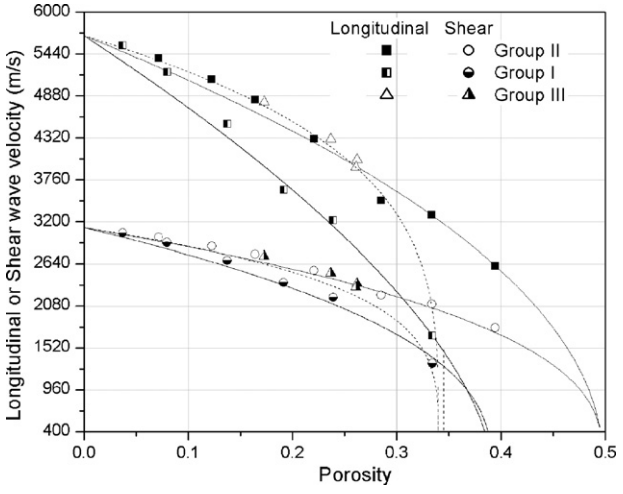

Fig. 3. Comparison of predicted shear moduli and Young's moduli with the experimental data.

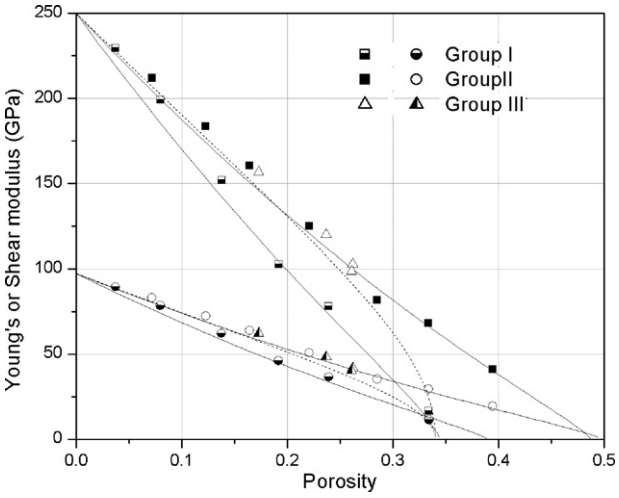

Fig. 4. Comparison of predicted bulk moduli with the experimental data.

and Young's modulus–porosity relation obtained from Eq. (12). The closeness of experimental bulk moduli calculated from the measured values of E and G to the predicted curves is remarkable, considering the sensitivity of these calculations to the propagation of experimental errors.

For a more rigorous test for the validity of Eq. (11) we compare the Poisson's ratio values calculated from the measured values of E and G with those predicted form Eq. (11), Eq. (5) and the Young's modulus–porosity relation obtained from Eq. (12). Fig. 5 shows the plot of the experimental and predicted ν versus porosity. The agreement between the predicted and the experimental values can be considered extremely good considering the fact that it is more prone to errors particularly at high values of porosity since it is calculated from the subtraction of two almost-equal terms.

Though the microstructures of the specimens were not reported, but Spinner et al.[1] had concluded that the higher rate of decrease of moduli in case of Group I specimens compared to that of the Group II specimens was due to the larger deviations of the pores of Group I specimens from sphericity compared to

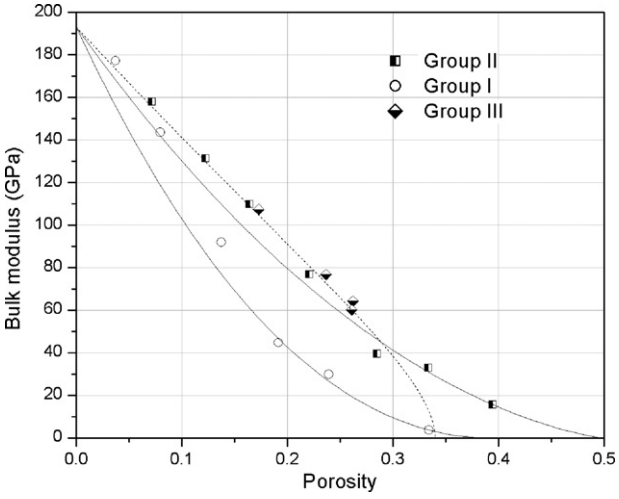

Fig. 5. Comparison of predicted Poisson's ratio with the experimental data.

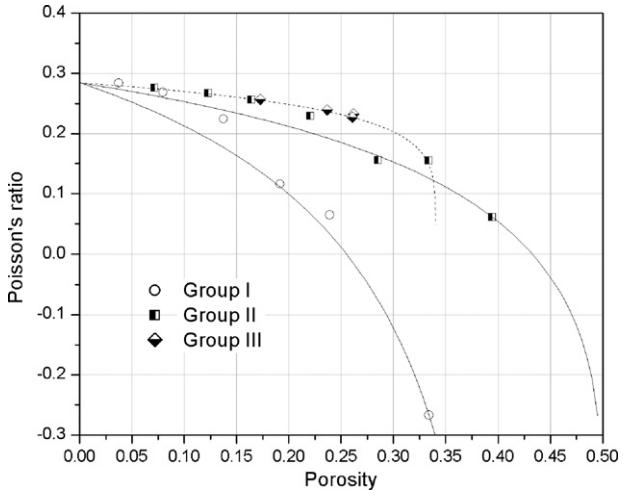

Fig. 6. Point-by-point calculation of optimum aspect ratio α fitting Mori–Tanaka theory to experimental modulus data.

that of Group II specimens. To ascertain the same, we calculated the value of the apparent spheroid aspect ratio giving the best fit to each experimental data point of all the specimens belonging to Groups I, II and III, by simultaneously minimizing the error between the moduli values predicted from Eqs. (1) and (2) and experimentally determined shear and bulk moduli. The function for error minimization is defined as follows:

$$\left[\frac{G_{\text{expt}} - G_{\text{theory}}(\alpha)}{G_{\text{expt}}}\right]^2 + \left[\frac{K_{\text{expt}} - K_{\text{theory}}(\alpha)}{K_{\text{expt}}}\right]^2 \quad (17)$$

where the subscripts expt and theory implies experimental and predicted data points, respectively. Fig. 6 shows the variation of the aspect ratio of all the group of specimens with porosity. The elastic moduli values calculated corresponding to these aspect ratios are shown in Figs. 3 and 4 with a + symbol. In all cases it shows excellent agreement with the experimental data.

4. Discussions

The above analysis is based on the proposed relation between the shear modulus and Young's modulus given by Eq. (11) which, on comparison with Eq. (7) derived on the basis of Mori–Tanaka approach, indicates that n_0 should not only depend on porosity, but also on pore morphology. Fig. 5 shows that the Groups I and II specimens have different pore morphologies as evident from different aspect ratio values and the respective values of $n_0 = 0.322$ and $n_0 = 0.501$ for these groups also seem to confirm the above. On the other hand, if we calculate the individual n_0 values for the four specimens of Group III which were prepared using 4–7 μm, 7–13 μm, 13–24 μm and 24–44 μm powders—the values work out to be 0.696, 0.691, 0.711 and 0.696, respectively. The specimens having powder size differing by an order of magnitude and pores of different aspect ratios (Fig. 5) yield identical values. It tends to indicate that the value of n_0 is independent of powder size and pore morphology and possibly dependent on some other material properties. Similar results are also obtained for alumina studied by Martin et al.[17]. They prepared three groups of specimens using powder sizes of 0.19 μm, 0.15 μm and 0.11 μm, respectively and measured the ultrasonic velocities. From these velocities, the E and G values have been calculated and the corresponding values of n_0 for three groups of specimens are evaluated as 0.843, 0.857 and 0.900, respectively which barely differ among themselves. Even the values of G for Groups I and II specimens, estimated from Eq. (11) using the values of $n_0 = 0.322$ and $n_0 = 0.501$, respectively, differ among themselves by not more than 2.65% on an average. Therefore, n_0 value for these groups, for all practical purposes, can be taken as the mean of the above two values, i.e. $n_0 = 0.412$ within the limits of experimental error. The solid line shown in Fig. 1 corresponds to Eq. (11) with $n_0 = 0.412$. Predicted values of G based on this mean value of n_0 agree with the experimental data with average deviations of 3.23% and 2.69% for Groups I and II specimens, respectively. However, the value of $n_0 = 0.412$ is much lower than the average value 0.699 for Group III specimens. A possible explanation for the same can be given as follows.

Eq. (11) relates two of the elastic moduli of a porous structure, namely the shear modulus, G, which describes the strain response of a body to shear stress or torsional stress, change of shape without change of volume and Young's Modulus, E, describing the strain response to an uniaxial stress or bending stress. It involves both volume change and shape change. Thus the relations between these two are expected be dependent on the stiffness of the porous structure. This will depend mainly on the particle morphology, average particle coordination number and the inter-particle contact geometry[18,19]. In this context, the evolution of the effective elastic behaviour of the powder compacts with the sintering history becomes important. Based on sintering studies of ceramic powders reported by several researchers[18,19], two distinct stages of sintering are noticed. In the first stage, sintering occurs by surface diffusion process with reduction in surface area and growth in inter-particle neck which leads to appreciable increase in the modulus values without any appreciable change in porosity level. During this stage, the relative moduli are function of average coordination number and neck/particle radius ratio[17,20,21]. In the intermediate stage of sintering, porosity is significantly reduced due to active bulk transport mechanism and neck growth. Both the initial and intermediate stages of sintering exhibit a characteristic linear relation between the surface area reduction and ultrasonic longitudinal wave velocity. Since specific surface area is directly related to the inter-particle neck morphology and the ultrasonic velocity is a function of the density and the elastic moduli[19], it can be inferred that the relative moduli will be a function of the neck morphology in the intermediate stage also. Thus it is the change in the neck morphology which determines the change in pore morphology and not vice versa. Therefore, it is also likely that the change in the neck morphology during sintering will be a dominant factor in determining the value of n_0. As the neck morphology is controlled directly by the sintering characteristics of the material, one may consider n_0 to be a material-dependent parameter.

For materials prepared without pore formers, the stiffness of the structure will be directly dependent on the neck/particle radius ratio. Thus Group III specimens which are free of pore

former exhibit a nearly constant n_0 indicating its dependence on the sintering characteristics alone. Introduction of pore formers will additionally weaken the structure which will not be related to the neck growth alone. Therefore, the Groups I and II specimens, in which the major percentages of pores have been introduced with pore formers, show a lower value of n_0. However, since their method of preparation is similar their n_0 values are very close to each other and the elastic behaviour of these two groups can be represented by a mean n_0 value.

Fig. 5 shows that the aspect ratio of pores of Group I specimens deviate more from spherecity than that of Group II specimens. This is in line with what Spinner et al.[1] have observed. However the rate of increase of aspect ratio with reduction in porosity for Group I specimens is faster than that of Group II specimens. This is possibly due to the faster sintering of smaller size powders in Group I specimens (0–2 μm) than that of Group II specimens (2–4 μm) as has also been observed by Martin et al.[17] for zinc oxide and alumina powders in the early stage of sintering. It may be further mentioned here that we have calculated the aspect ratio of all the individual Groups I and II specimens and estimated the moduli from the self-consistent theory of Mori–Tanaka[13] which agrees extremely well with the measured values. However, our attempt to estimate the moduli based on an "effective aspect ratio" as defined by Dean[11], based on this theory failed.

5. Conclusion

Elastic moduli versus porosity relation of polycrystalline thoria has been reanalyzed in the light of the Mori–Tanaka mean field approach. A relation between the shear modulus and Young's modulus of porous polycrystalline thoria has been derived. It shows that for materials without artificial pore formers, the variation of the shear modulus with Young's modulus is possibly dependent on its sintering characteristics rather than pore morphology. Assuming a power law type dependence of moduli on porosity, a new method has been suggested for predicting variation of elastic moduli with porosity based on experimental data at a single porosity only.

Acknowledgement

The authors thank Director, CGCRI for his permission to publish this paper.

References

1. Spinner, S., Knudsen, F. P. and Stone, L., Elastic constant–porosity relations for polycrystalline thoria. *J. Res. Natl. Bur. Std., Sect. C*, 1963, **67C**, 39–46.
2. Dewey, J. M., The elastic constants of materials loaded with non-rigid fillers. *J. Appl. Phys.*, 1947, **18**, 578–581.
3. Mackenzie, J. K., The elastic constants of a solid containing spherical holes. *Proc. Phys. Soc. Lond. B*, 1950, **63**, 2–11.
4. Kerner, E. H., The elastic and thermo-elastic properties of composite media. *Proc. Phys. Soc. Lond. B*, 1956, **69**, 808–813.
5. Gatto, F., Influence of small cavities on velocity of sound in metals. *Allumonio*, 1956, **19**, 19–26.
6. Hashin, Z., The elastic moduli of heterogeneous materials. *J. Appl. Mech.*, 1962, **29**, 143–150.
7. Zaunzemis, W., *Continuum Mechanics*. Macmillan, New York, 1987, pp. 344–46.
8. Rothenburg, L., Berlin, Al. and Bahrust, R. J., Microstructure of isotropic materials with negative Poisson's ratio. *Nature*, 1991, **354**, 470–472.
9. Hanna, R. K. and Crandell, W. B., Elastic and anelastic properties of MgO. *Am. Ceram. Soc. Bull.*, 1962, **41**, 311 (abstract).
10. Yeheskel, O., Ratzker, M., Shokhat, M. and Dariel, M. P., Elastic constants of porous silver compacts after acid assisted consolidation at room temperature. *J. Mater. Sci.*, 2001, **36**, 1219–1225.
11. Dean, E. A., Elastic moduli of porous sintered materials as modeled by a variable-aspect-ratio self-consistent oblate-spheroidal-inclusion theory. *J. Am. Ceram. Soc.*, 1983, **66**, 847–854.
12. Wu, T. T., The effect of inclusion shape on the elastic modulus of a two-phase material. *Int. J. Solid Struct.*, 1966, **3**(1), 1–8.
13. Mori, T. and Tanaka, K., Average stress in matrix and average elastic energy of materials with misfitting inclusions. *Acta Metall.*, 1973, **21**, 571–574.
14. Dunn, M. L. and Ledbetter, H., Poisson's ratio of porous and microcracked solids: theory and application to oxide superconductors. *J. Mater. Res.*, 1995, **10**(11), 2715–2722.
15. Phani, K. K., Elastic-constant–porosity relations for polycrystalline thoria, 1986, **5**, 747–750.
16. Macedo, P. M., Capps, W. and Wachtman Jr., J. B., Elastic constants of single crystal ThO_2 at 25 °C. *J. Am. Ceram. Soc.*, 1964, **47**, 651.
17. Martin, L. P., Nagle, D. and Rosen, M., Effect of particle size distribution upon specific surface area and ultrasonic velocity in sintered ceramic powders. *Mater. Sci. Eng.*, 1998, **A246**, 151–160.
18. Green, D. J., Nader, C. and Brezny, R., The elastic behaviour of partially-sintered alumina. *Ceram. Trans.*, 1990, **7**, 345–356.
19. Martin, L. P. and Rosen, M., Correlation between surface area reduction and ultrasonic velocity in sintered zinc oxide powders. *J. Am. Ceram. Soc.*, 1997, **80**(4), 839–846.
20. Boonyongmaneerat, Y., Mechanical properties of partially sintered materials. *Mater. Sci. Eng. A*, 2007, **452–453**, 773–780.
21. Arato, P., Besenyei, E., Kele, A. and Weber, F., Mechanical properties in the initial stage of sintering. *J. Mater. Sci. Lett.*, 2000, **19**, 1557–1558.